Structural Basis for the Design of Antibiotics Targeting Peptide Deformylase[†,‡]

Bing Hao, Weimin Gong, P. T. Ravi Rajagopalan, Ying Zhou, Dehua Pei, and Michael K. Chan*

Departments of Biochemistry and Chemistry, The Ohio State University, 484 West 12th Avenue, Columbus, Ohio 43210

Received October 30, 1998; Revised Manuscript Received February 4, 1999

ABSTRACT: While protein synthesis in bacteria begins with a formylated methionine, the formyl group of the nascent polypeptide is removed by peptide deformylase. Since eukaryotic protein synthesis does not involve formylation and deformylation at the N-terminus, there has been increasing interest in peptide deformylase as a potential target for antibacterial chemotherapy. Toward this end and to aid in the design of effective antibiotics targeting peptide deformylase, the structures of the protein−inhibitor complexes of both the cobalt and the zinc containing *Escherichia coli* peptide deformylase bound to the transition-state analogue, (*S*)-2-*O*-(H-phosphonoxy)-L-caproyl-L-leucyl-*p*-nitroanilide (PCLNA), have been determined. The proteins for both deformylase−inhibitor complexes show basically the same fold as for the native enzyme. The PCLNA inhibitor adopts an extended conformation and fits nicely into a hydrophobic cavity located near the metal site. On the basis of these structures, guidelines for the design of high-affinity deformylase inhibitors are suggested. As our results show that the protein residues which interact with the PCLNA inhibitor are conserved over a wide variety of species, we suggest that antibiotics targeting deformylase could have wide applicability.

In prokaryotes, protein synthesis begins with a formylated methionine, N-formylmethionine (fMet)[1] (*1*). Following translation initiation, the formyl group at the N-terminus of the growing polypeptide is removed by peptide deformylase (PDF) (*2*−*4*). The deformylation process is necessary to obtain the final mature protein and is essential for bacterial survival (*5*). As cytoplasmic protein synthesis in eukaryotic cells does not use fMet in translation initiation, it has been proposed that specific deformylase inhibitors could selectively block the growth of bacterial cells with minimal toxicity to a eukaryotic host (*5*, *6*). The identification and structural determination of suitable inhibitors bound to deformylase would facilitate both the elucidation of the deformylation mechanism and the design of powerful therapeutic tools.

PDF is a novel metallopeptidase which has been recently shown to utilize iron as the catalytic metal for amide hydrolysis (*6*). Biochemical or structural characterization of the iron form of the enzyme, however, has been hampered by its extreme instability. Through in vitro reconstitution or overexpression in bacterial cells, the iron metal can be replaced by zinc (*6*, *7*), nickel (*8*), or cobalt (P. T. R. Rajagopalan and D. Pei, unpublished results) to give stable variants that retain partial (Zn form) or nearly full catalytic activity (Ni and Co forms). We and others have previously reported the three-dimensional structures of the zinc (*9*, *10*) and nickel (*8*, *11*) containing *Escherichia coli* PDF. No significant differences in either the overall or active-site structure were observed for either form. In each of these structures, the metal ion adopts a tetrahedral geometry formed by two histidine residues from a conserved HEXXH motif, a cysteine residue from a conserved EGCLS motif, and a water molecule (or hydroxide ion). These structures have yielded the first insights into the overall structure of deformylase and have provided a structural basis to address the mechanistic issues of the deformylation reaction.

In light of the key role that PDF plays in prokaryotic protein synthesis and its potential application to antibacterial chemotherapy, we have been interested in the design and structural determination of high-affinity deformylase inhibitors. In this paper, we present the three-dimensional crystal structures of the cobalt and zinc containing PDF complexed with a transition-state analogue, (*S*)-2-*O*-(H-phosphonoxy)-L-caproyl-L-leucyl-*p*-nitroanilide (PCLNA) (*12*). The design of PCLNA is based on the structure of a potent substrate, f-Met-Leu-*p*-nitroanilide (*13*), and incorporates an additional H-phosphonate group to mimic the tetrahedral intermediate implicated during formyl hydrolysis. L-Caproyl was utilized in place of L-methionine to facilitate its synthesis. PCLNA acts as a competitive inhibitor of both the zinc and iron forms of PDF with K_I values of 76 and 37 μM, respectively (*12*). These are the first structures of PDF bound to a inhibitor that mimics the physiological substrate. The structures of these PDF−PCLNA complexes are compared with the unliganded zinc form, and this information will be utilized to map out the important protein−substrate interactions that could be critical for the design of new antibiotics.

MATERIALS AND METHODS

Isolation and Crystallization. E. coli PDF was purified as previously described (*7*). The PCLNA inhibitor was chemi-

[†] This work was supported by funds from the Ohio State University, the Petroleum Research Fund (30850-G3 to M.K.C.), and the NIH (AI40575 to D.P.).

[‡] The coordinates have been deposited in the Protein Data Bank. PDB filenames: 1BSJ (cobalt) and 1BSK (zinc).

* To whom correspondence should be addressed.Phone: 614-292-8375. Fax: 614-292-6773. E-mail: chan@chemistry.ohio-state.edu.

[1] Abbreviations: PDF, peptide deformylase; PCLNA, (*S*)-2-*O*-(H-phosphonoxy)-L-caproyl-L-leucyl-*p*-nitroanilide; fMet, *N*-formylmethionine; *p*-NA, *p*-nitroanilide.

10.1021/bi982594c CCC: $18.00
Published on Web 03/27/1999

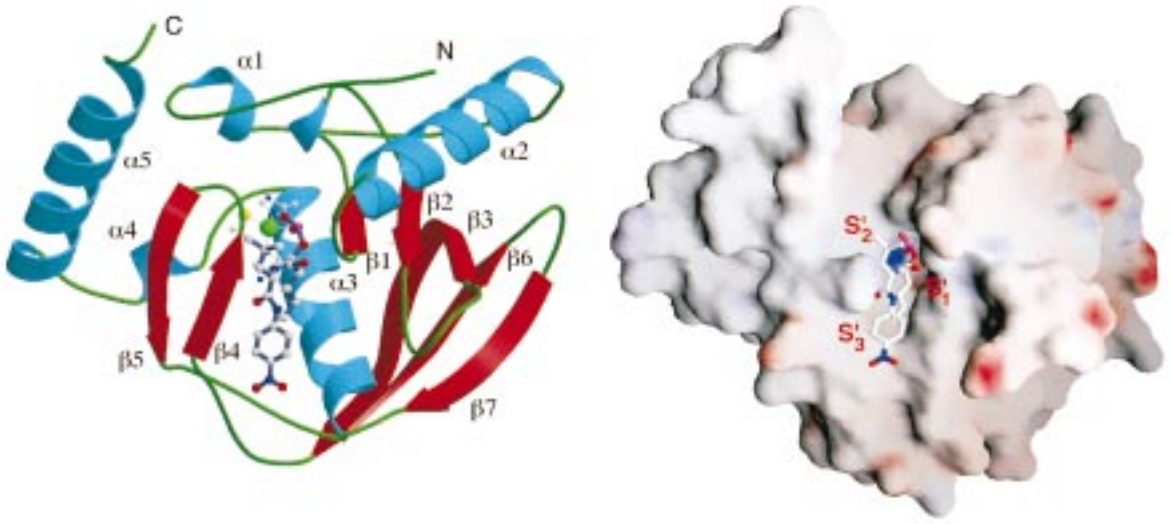

FIGURE 1: (a, left) Ribbons diagram of the *E. coli* PDF−PCLNA complex as viewed toward the substrate cleft. The secondary structures are color-coded with α helical regions as light blue, *β*-sheet regions as red, and the remainder as green. The metal and inhibitor are colored by element, with carbon as gray, nitrogen as blue, oxygen as red, phosphorus as magenta, and the metal ion as green. (b, right) Electrostatic potential surface of the PDF protein and stick diagram of the PCLNA inhibitor prepared using the program GRASP (*26*).

cally synthesized as reported (*12*). Crystals of both cobalt and zinc PDF−PCLNA complexes were grown using hanging drop vapor diffusion method at 4 °C. The reservoir solution contained 1 mL of 0.1 M Tris-HCl buffer (pH 8.5) and 1.9 M $NH_4H_2PO_4$. Equal volumes of reservoir solution and protein solution [14.4 mg/mL protein, 20 mM NaH_2PO_4 buffer (pH 7.0), 10 mM NaCl, 0.86 M $(NH_4)_2SO_4$, and 1 mM inhibitor] were mixed. Prior to data collection, the crystals were treated stepwise with mother liquor solutions containing increasing amounts of glycerol up to a final concentration of 40% (v/v). The crystals were then mounted on nylon loops and then cooled to 100K under a stream of nitrogen.

Data Collection and Processing. X-ray diffraction data were collected at Beamline X4A of the National Synchrotron Light Source, Brookhaven National Laboratory, using a RAXIS 100 detector. Autoindexing and scaling were done with version 1.9 of the HKL program suite (*14*). The cobalt PDF−PCLNA complex crystal diffracted to 2.1 Å resolution with cell dimensions of $a = b = 98.38$ Å, $c = 109.37$ Å, $\alpha = \beta = 90.0°$, and $\gamma = 120.0°$. The zinc PDF−PCLNA complex crystal diffracted to 2.4 Å resolution with cell dimensions of $a = b = 100.11$ Å, $c = 111.34$ Å, $\alpha = \beta = 90.0°$, and $\gamma = 120.0°$. The systematic absences indicated that the space group was either $P6_122$ or $P6_522$. Each unit cell contained one PDF−PCLNA complex per asymmetric unit.

Structure Determination and Refinement. The two *E. coli* PDF−PCLNA complex structures were solved by the molecular replacement method using the program X-PLOR version 3.851 (*15*). The 2.9 Å refined model of the native zinc *E. coli* PDF (*10*) was used as an initial search model over the resolution range 12−3.0 Å. The correct solution for each was the highest peak in the rotation and translation search in the space group $P6_522$. The refinement was performed with X-PLOR, using standard protocols and solvent correction (*15*). Modeling of the electron density was done using the program O (*16*). The structure of the PCLNA inhibitor was determined based on $2F_O - F_C$ and $F_O - F_C$ maps. The *R* factor of the final model for the cobalt PDF−PCLNA complex was 19.9% ($R_{free} = 22.8\%$) and for the zinc PDF−PCLNA complex was 19.9% ($R_{free} = 22.3\%$) (*17*). Figures were prepared with the programs XtalView (*18*), MOLSCRIPT (*19*), and Raster 3D (*20*).

Table 1: Data Processing Statistics

	cobalt	zinc
space group	$P6_522$	$P6_522$
cell parameters	$a = b = 98.38$ Å, $c = 109.37$ Å	$a = b = 100.11$ Å, $c = 111.34$ Å
molecules in asymmetric unit	1	1
effective resolution (Å)	20.0 −2.1 Å	20.0−2.4 Å
number of reflections	118 933	58 431
number of unique reflections	16 692	10 960
R_{merge} (%)[a,b]	7.4 (23.6)	7.9 (24.0)
completeness (%)[b]	87.3 (87.7)	85.2 (86.3)

[a] $R_{merge}(I) = \sum_h \sum_i |I_i - I| / \sum_h \sum_i I$, where I is the mean intensity of the i observations of reflection h. [b] The numbers in parentheses are for the highest resolution shell (2.19−2.10 Å for the cobalt data and 2.48−2.40 Å for the zinc data).

RESULTS AND DISCUSSION

The Protein. The structures of both the cobalt and zinc PDF−PCLNA complexes are virtually identical. The zinc form is shown in Figure 1a. Each model contains the PCLNA peptide inhibitor, solvent water molecules, and the protein molecule containing 166 out of a total of 168 amino acid residues. The last two C-terminal residues were not observed. The crystallographic data and refinement statistics are listed in Tables 1 and 2.

Both PDF−PCLNA complexes retain essentially the same fold as the native zinc PDF structure. The rms deviation between the Cα atoms of the zinc PDF and the zinc PDF−PCLNA complex is 0.50 Å. Superposition of these structures reveals that the only significant main-chain conformational change occurs in the loop region between *β*-strand II and *β*-strand III (residues Val-62 to Glu-68). In light of its distance from the active site (18.5 Å), this conformational change is unlikely to be due to inhibitor binding, but most

Table 2: Refinement Statistics

	cobalt	zinc
Refinement		
no. of scattering atoms		
protein	1330	1330
inhibitor	29	29
metal	1	1
solvent molecules	100	76
resolution range	20.0−2.1	20.0−2.4
reflections used	16 692	10 960
R factor (%)[a]	19.9	19.9
R_{free} (%)[b]	22.8	22.3
Model Geometry		
rms deviation		
bond distance (Å)	0.014	0.015
bond angles (deg)	1.594	1.739

[a] R factor = $100 \times \sum|F_{obs} - F_{calc}|/\sum|F_{obs}|$, where F_{obs} and F_{calc} are the observed and calculated structure factors, respectively. [b] R_{free} was calculated using 8% of the reflections.

likely arises from crystal-packing forces. In the PDF−PCLNA complex crystal, this loop contacts the side chains of Arg-109, Lys-106, and Glu-119 of another symmetry-related PDF molecule. In the zinc native crystals, due to the different space group and unit cell, this loop is exposed to the solvent.

The secondary structure assignments for the zinc PDF−PCLNA complex as determined by PROCHECK (*21*) and DSSP (*22*) are (using the same labeling scheme as for the native structure) α-helix, (I) 11−14, (II) 25−40, (III) 124−137, (IV) 142−145, (V) 148−163; β-strand, (I) 45−47, (II) 57−60, (III) 70−81, (IV) 87−90, (V) 93−99, (VI) 105−111, (VII) 117−122 and 3_{10} helix, 49−51. Overall, these assignments are identical to the zinc native structure. The cobalt PDF−PCLNA complex has similar secondary structure assignments except that β-strands IV and V are each three residues longer: residues 84−90 and residues 93−102, respectively. Analysis of these regions reveals no significant differences in their structures and these assignments appear to differ in different models generated at different resolutions. The variation of the secondary structure assignments within this region may be due to the arbitrary cutoff value in the secondary structure prediction algorithm and as such our assignments are based on the zinc model.

As was reported for the native nickel PDF structure (*8*), Pro-9 could be best modeled as *cis*-proline in both PDF−PCLNA complex structures. This had been previously defined as a *trans*-proline in our native zinc PDF structure (*10*). Reanalysis of the $F_O - F_C$ density indicates that Pro-9 is a *cis*-proline in the native zinc PDF structure as well.

The Inhibitor. Our main interest in the structure of the PDF−PCLNA complex is to elucidate the interactions which contribute to the binding affinity of inhibitors. Such information is critical for the further design of more potent inhibitors. The location and orientation of the PCLNA inhibitor have been determined from the $F_o - F_c$ and $2F_o - F_c$ maps and reveal that it adopts a β-strand conformation (Figure 2). The PCLNA inhibitor inserts into a cleft formed by the active-site helix (125−136) on the bottom, the β-strand I (43−47) on one side, the β-strand IV (87−91) on the other side, and the 3_{10} helix at the back. This binding pocket is similar to that determined from the interaction of poly(ethylene glycol) at the active site (*8*).

In light of the fact that the deformylase active site resides in a hydrophobic cleft, one important factor contributing to the binding affinity of the PCLNA inhibitor may be its ability to fill the hydrophobic cavity (Figure 1b). Enhanced protein stability has been shown to be associated with removal of cavities, resulting from the reduction of the unfavorable surface energy and the increase of the favorable hydrophobic packing contacts. Calculations of the solvent-accessible surface areas of the native deformylase protein (8,350 Å^2), the PCLNA inhibitor (700 Å^2), and the PDF−PCLNA complex (8,210 Å^2) using X-PLOR reveal that the binding of the PCLNA inhibitor to PDF results in a lower molecular surface area for the protein in general, burying a total of 840 Å^2 of surface area (*15*, *23*). These results support the potential importance of these effects on the PCLNA binding affinity.

As PCLNA is a peptide-based transition-state analogue, our structures of the PDF−PCLNA complexes also allow

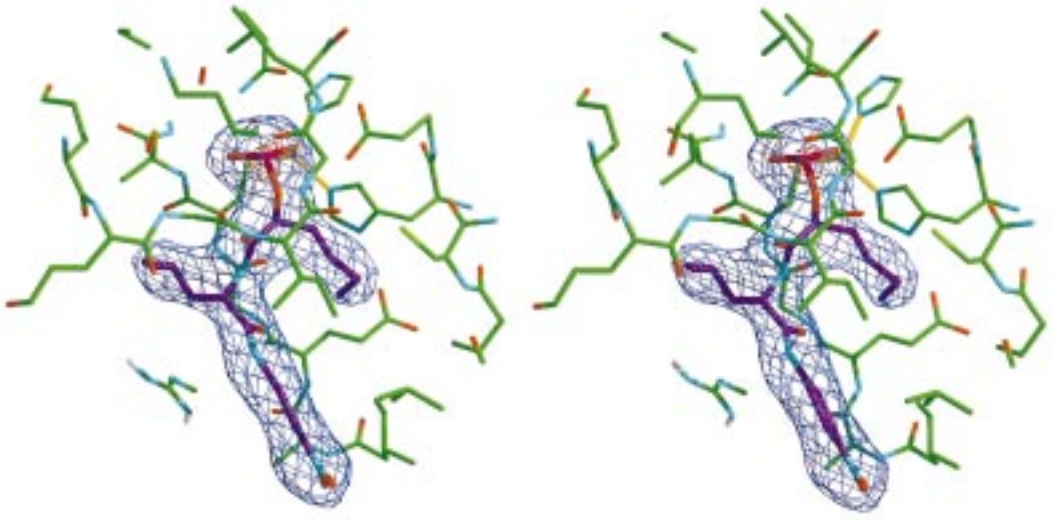

FIGURE 2: Stereoview of the $F_O - F_C$ electron density map of the active site with the inhibitor omitted (blue, 5σ density; red, 15σ density). The Cα atoms of protein are colored in brown, while those for the inhibitor are colored in purple. The remaining atoms are colored by element, nitrogen as cyan, oxygen as red, phosphorus as magenta, sulfur as yellow, and the metal ion as green.

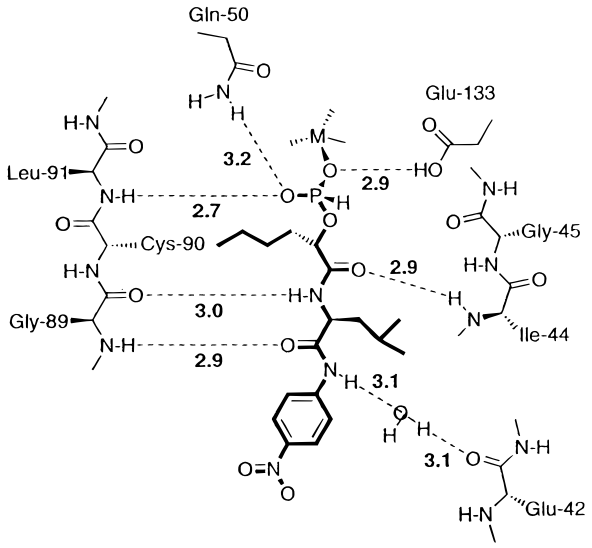

FIGURE 3: Protein−inhibitor hydrogen-bonding interactions within the zinc PDF−PCLNA complex. The hydrogen-bonding distances for the cobalt containg enzyme are comparable within ±0.2 Å.

for an understanding of how PDF recognizes nascent peptides, its physiological substrate, and mediates the hydrolysis of the N-formyl peptide bond. One important global feature relevant to the binding of the PCLNA inhibitor may be our observation that the PCLNA peptide, together with β-strands IV and V from the PDF protein, form an antiparallel β-sheet. Three hydrogen bonds are formed between the main-chain atoms of the inhibitor and the β-strand IV of the protein (Figure 3). The formation of this sheet involves

Table 3: Interactions between Inhibitor and Protein

inhibitor binding site	residues forming the binding site[a]
H-phosphonate	Q50, L91, E133
S_1'	G43, I44, G45, E88, C129, H132, E133
S_2'	E42, G43, G89, L91
S_3'	I44, I86, E87, L125, G′124, L′125, I′128

[a] Residues located within 4.0 Å of the inhibitor are listed.

cooperative interactions and likely contributes significant stability to the peptide binding affinity. These considerations suggest a potential role for these specific secondary structural elements within the PDF protein.

There are, of course, other important interactions involving individual residues of the PCLNA inhibitor and the PDF protein (Table 3). For instance, the *p*-nitroanilide (*p*-NA) group at the C-terminal end of the PCLNA inhibitor (S_3', farthest from the metal ion) has been shown to be critical for binding (*13*). For example, f-Met-Leu-*p*-nitroanilide is a potent substrate of the *E. coli* iron PDF (k_{cat} of 38 s^{-1}, a K_M of 20 μM, and a k_{cat}/K_M of 1.9×10^6 M^{-1} s^{-1}). Removal of the C-terminal *p*-NA group reduces the enzyme's affinity to f-Met-Leu-NH_2 by ~40-fold ($k_{cat} = 194$ s^{-1}, $K_M = 840$ μM, $k_{cat}/K_M = 2.3 \times 105$ M^{-1} s^{-1}). However, the mapping of the interactions of the *p*-NA group with the PDF protein in the present study is complicated by the fact that the *p*-NA also interacts with a symmetry-related molecule generated by a crystallographic 2-fold located near the active site. As a result, the *p*-NA of the PCLNA inhibitor interacts with residues from both the protein to which it is bound as well as residues from the symmetry-related protein. One face of

FIGURE 4: Sequence alignment of the PDF residues which form the substrate binding site. The residues involved are colored by the region of the inhibitor they interact with: H-phosphonate (violet), L-caproyl (blue), L-leucine (green), and nitrophenylaniline (yellow). The color is alternated for those residues which interact with more than one region. The sequences were obtained from the EBI databases (http://www.ebi.ac.uk/dbases/topdata.html) and were aligned using the GCG package (Wisconsin Package Version 9.0, Genetics Computer Group (GCG), Madison WI).

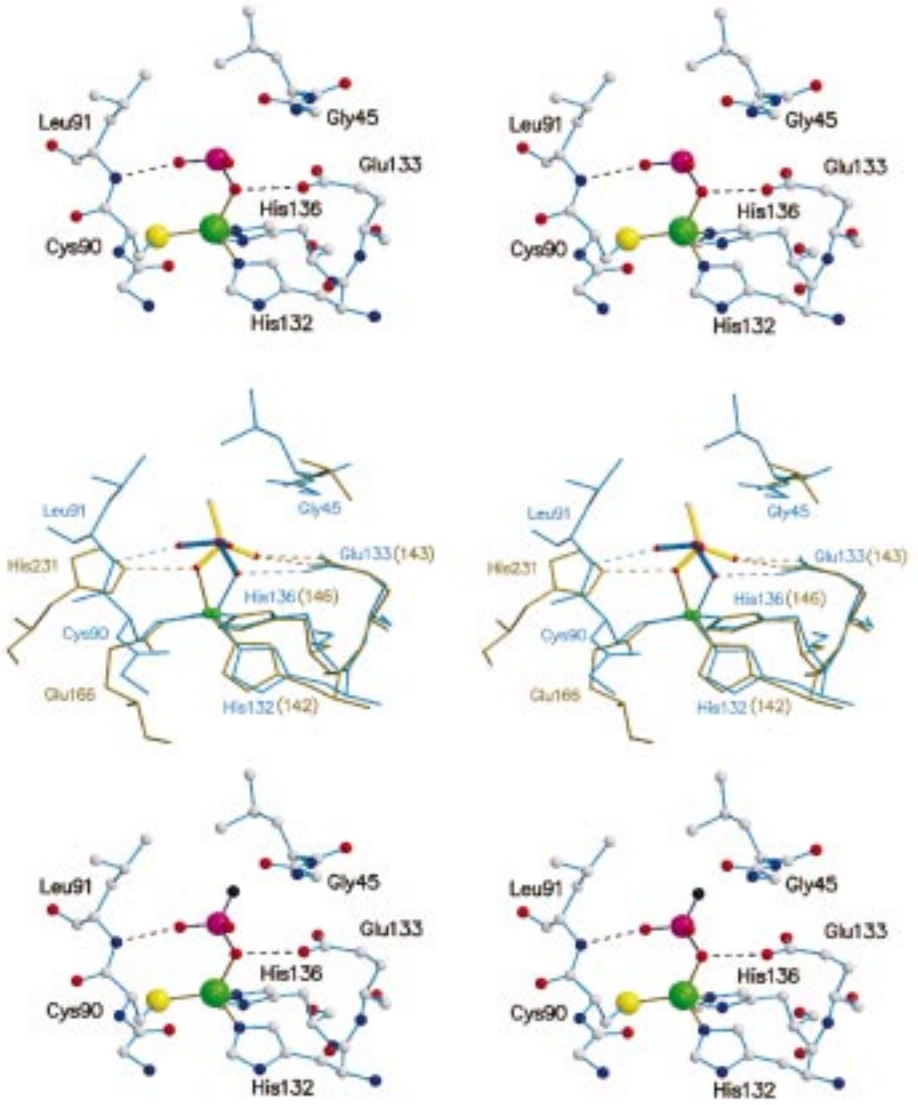

FIGURE 5: (top) Stereoview of the structure of the active site of the zinc PDF−PCLNA complex. Hydrogen-bonds are indicated by dashed lines. The atoms are colored by element as in Figure 1a. (middle) Superimposed stereoview diagram of the structures and interactions of phosphonate inhibitors bound to thermolysin (brown) and PDF (blue). The inhibitors of thermolysin and PDF are colored as light yellow and dark blue, respectively. The thermolysin coordinates were obtained from the Protein Data Bank (PDB file 6TMN). (bottom) Hypothetical model for the transition state involved in the deacylation of acetylated peptides to illustrate the steric interaction of a methyl group (black) with the backbone carbonyl.

the hydrophobic pocket around the bound *p*-NA group is formed by the side chains of three protein residues, Ile-44, Ile-86, and Leu-125, the backbone carbonyl of Glu-87, and the caproyl side chain of the PCLNA inhibitor itself. The other side of the *p*-NA group is in close contact with the backbone and/or side chains of Gly′-124, Leu′-125, and Ile′-128 of the symmetry-related protein. While there are undoubtedly additional interactions which stabilize the protein−protein interface between the two molecules, no other experiments we have performed to date support the presence of a dimer in solution.

The second residue of the PCLNA inhibitor, L-leucine (S_2'), is in van der Waals contact with Leu-91 and the main-chain carbonyl groups of residues Glu-42 and Gly-43 on one side, while the other side is exposed to solvent. The backbone amide and carbonyl of the leucyl residue are also hydrogen-bonded to the corresponding carbonyl and amide of Gly-89. These interactions are to be expected when the peptide is involved in the formation of an antiparallel β-sheet. Since the side chain of this group is directed toward an open cavity, as shown in Figure 1b, the enzyme should be able to accommodate a number of different amino acids at this position.

The N-terminal L-caproyl group (S_1', closest to the metal ion), which mimics the methionine amino acid, sits in a pocket generated by residues Gly-43, Ile-44, Gly-45, Glu-88, Cys-129, His-132, and Glu-133, as well as the *p*-NA group of the PCLNA inhibitor itself. The carbonyl of the caproyl group is hydrogen bonded to the main-chain amide nitrogen of Ile-44. The most interesting feature, however, involves the caproyl group and the *p*-NA group. As a result of the β-strand conformation of the PCLNA inhibitor, the *p*-NA group acts as a lid, burying the caproyl side chain in a hydrophobic cleft of the protein. These intimate hydrophobic interactions between the protein and the inhibitor no doubt contribute in an important way to the binding affinity of this inhibitor and provide a potential explanation for the enzyme's strong preference for a methionine residue at the N-terminus of peptide substrates (*7*).

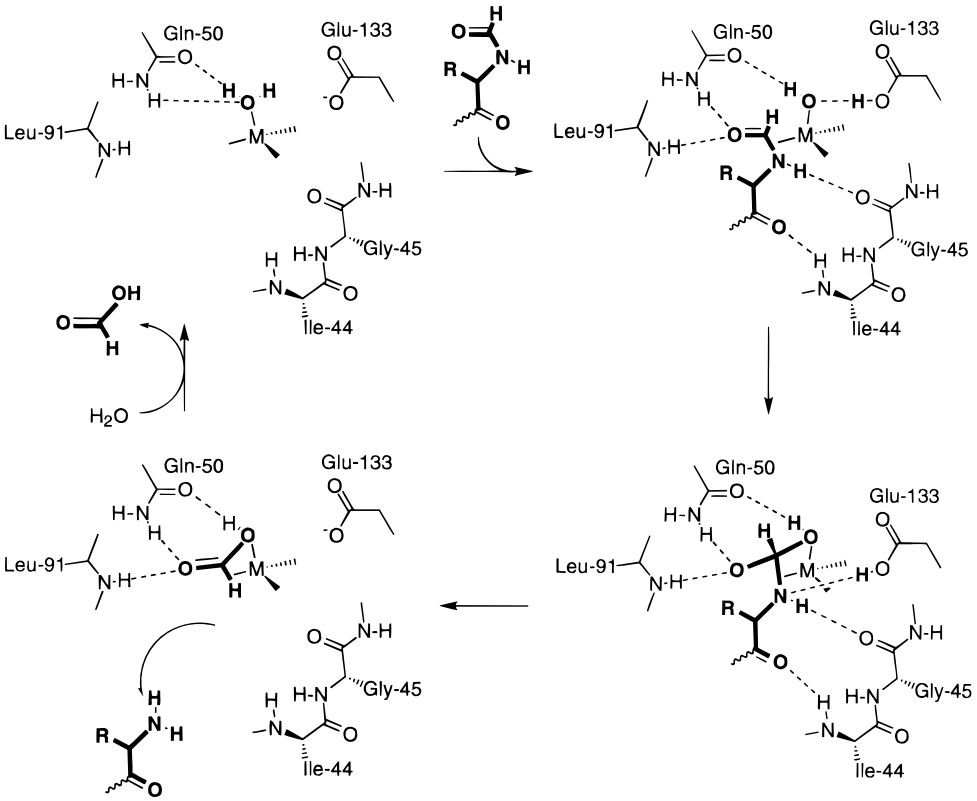

FIGURE 6: Proposed mechanism of PDF based on the native (top, left) and complex (bottom, right) structures.

Finally, the H-phosphonate moiety of the PCLNA inhibitor also provides important interactions. As expected, this group binds to the zinc metal using one of its phosphonate oxygens, replacing the water in the native structure. Glu-133 also forms a hydrogen bond to the phosphate oxygen that binds the metal, consistent with its potential importance in the catalytic mechanism (Figure 5, top). Glu-133 is thought to act as a proton shuttle, receiving the proton from the metal bound water and then donating it to the amide NH to facilitate bond cleavage. The carbonyl group of Gln-50 is within hydrogen-bonding distance (3.1 Å) of this phosphonate oxygen as well. In the native protein, this carbonyl group could be used to stabilize the metal hydroxide.

The second phosphonate oxygen of the inhibitor, which mimics to the carbonyl oxygen of the formyl group in the enzyme−substrate complex, forms hydrogen bonds to the main-chain amide NH of Leu-91 and the side-chain amide NH2 of Gln-50. The third phosphonate oxygen, whose position would correspond to the N-terminal methionine amide nitrogen of nascent peptides, is not involved in a hydrogen bond in the PDF−PCLNA complex. However, it is within hydrogen-bonding distance (3.1 Å) of the carbonyl of Gly-45. Presumably, in the physiological reaction, the formylated N-terminal amide NH of the nascent peptide hydrogen bonds to this carbonyl group.

All total, in addition to hydrophobic and metal binding interactions, the PDF−PCLNA complex structure reveals seven hydrogen bonds that could account for the structure of the bound inhibitor in the enzyme and its binding affinity (Figure 3). An important issue in the design of antibiotics is, of course, the generality of these interactions over different organisms. Figure 4 summarizes the results of sequence analysis of the residues which must interact with the PCLNA inhibitor (within 4.0 Å) over PDF proteins from a wide variety of organisms given the mode of inhibition inferred from the present study. The important result is that these residues are highly conserved among all PDF proteins, including those with low overall sequence homology. This outcome is not unexpected in light of the generality of the deformylation reaction, and it suggests that drugs targeting PDF will have broad applicability.

Implications on the Catalytic Mechanism. Previously, we compared the structure of the native zinc PDF with a thermolysin−inhibitor complex (*24*). With our present structure of the zinc PDF−PCLNA complex, a new comparison is now possible and is depicted in Figure 5 (middle). While both inhibitors contain a bound phosphonate, one surprising result is that the orientation of the phosphonate is different between the PDF−PCLNA and thermolysin−inhibitor complexes. In the PDF−PCLNA complex, the phosphonate oxygen, which does not bond to the metal, forms a hydrogen bond with the backbone amide NH of Leu-91. For all other related metalloproteases bound to phosphonate inhibitors that we have analyzed, this phosphonate oxygen hydrogen bonds the catalytic glutamate (Glu-143 in thermolysin, Glu-133 in *E. coli* PDF). Thus, there is a subtle difference in the orientation of the transition state within the active site of these metalloproteases.

The different orientation of the transition-state analogue may be used to support the notion that PDF represents a new class of metalloprotease. More importantly, however, these structural details yield insight into its catalytic mechanism. Previously, we have suggested that PDF utilizes a hydrolytic mechanism in which a metal-bound hydroxide attacks the formyl group. In many hydrolytic enzymes, however, a Lewis acid mechanism has been suggested in which the metal ion is used to activate the amide bond. On the basis of the orientation of the transition-state analogue,

however, the mechanism of PDF appears clear. Because the Leu-91 amide NH can only act as a Lewis acid and not as a base, the nucleophilic hydroxide must come from the metal. Our observation that the Leu-91 amide NH hydrogen bonds to the phosphonate suggests that the NH group acts as a Lewis acid which helps to activate the formyl oxygen.

In summary, it is clear that our present structures of the native PDF and the PDF−PCLNA complex bound to the transition-state inhibitor, PCLNA, have helped to clarify the catalytic mechanism of the deformylase protein. On the basis of these structures, we now propose a revised mechanism for the deformylation by PDF shown in Figure 6. Further work to address other critical issues of this mechanism is underway.

The Origin of the Specificity for N-Formylated Peptides. Biochemical studies have revealed that while PDF efficiently deformylates peptides containing an N-terminal fMet, it is much less active toward the corresponding *N*-acetyl-Met-peptides. These observations have been one of the intriguing issues regarding this enzyme. On the basis of the structure of the PDF−PCLNA complex structure, we have modeled the transition state for deacylation of *N*-acetylated peptides, by replacing the proton on the H-phosphonate group with a methyl group (Figure 5, bottom). This analysis revealed that the modeled methyl group forms a close interaction (2.2 Å) with the carbonyl oxygen of Gly-45, one of the potentially important residues involved in the catalytic mechanism. This steric interaction would hinder the deacylation of acetylated substrates. Thus, *E. coli* PDF may have evolved to use the altered orientation of the transition state to achieve its catalytic selectivity.

CONCLUSIONS

Our fundamental interest in PDF stems from its potential as a target for antibacterial chemotherapy. Indeed, the PDF−PCLNA complex structure offers certain guidelines for the design of high-affinity PDF inhibitors. First, at the S_1' site, a hydrophobic side-chain analogous to methionine appears to be important to fill a hydrophobic pocket. Second, a large aromatic group is needed at the S_3' position to help to bury the hydrophobic S_1' residue. Third, the side chains of the S_2' residue do not make extensive interactions with the protein and, therefore, it seems likely that a variety of groups could be tolerated at this position. Finally, a small group capable of binding to the metal ion and/or forming hydrogen bonds with other active-site residues could be exploited to provide additional binding energy.

Our structures of the PDF−PCLNA complexes also address some basic questions concerning the mechanism of action of PDF. A classical question in metallopeptidase catalysis is the function of the metal, which can either bind to the carbonyl oxygen and activate the peptide bond for nucleophilic attack or bind a water molecule and promote the formation of a more nucleophilic metal bound hydroxide. The two PDF−PCLNA complex structures strongly support the metal hydroxide mechanism. On the basis of the details of the binding of the phosphonate transition-state analogue, we surmise that, in the tetrahedral intermediate required for deformylation, the oxygen bound to the metal is derived from the water, whereas the oxygen hydrogen bonded to the amide NH of Leu-91 originates from the formyl group of the formylated peptide. Metal-based Lewis acid catalysis appears less likely since the nucleophilic water is distant from Glu-133, the most likely catalytic base essential for PDF activity (*25*).

Finally, the present structural study of the PDF−PCLNA complex has provided clues into the origin of specificity of PDF proteins for formylated peptides over acetylated substrates. On the basis of the orientation of the H-phosphonate transition-state analogue in the active site, the additional methyl group in acetylated substrates would interfere sterically with the backbone carbonyl of Gly-45 upon formation of the tetrahedral intermediate. In contrast, formylated peptides would direct a proton into this region.

ACKNOWLEDGMENT

We thank Professor Muttaiya Sundaralingam for the use of his RAXIS machine in our initial crystal screening experiments, Dr. Craig Ogata for beamline assistance at the X4A beamline of the National Synchrotron Light Source, Brookhaven National Laboratory, and Dr. Yun-Jin Hu for preparation of the PCLNA inhibitor. X4A beamline at the National Synchrotron Light Source, a Department of Energy facility, is supported by the Howard Hughes Medical Research Institute. The initial molecular replacement solution was determined by Weimin Gong while he was still a postdoctoral research fellow in Dr. Xiaodong Cheng's laboratory of Emory University.

REFERENCES

1. Kozak, M. (1983) *Microbiol. Rev. 47*, 1−45.
2. Adams, J. M. (1968) *J. Mol. Biol. 33*, 571−589.
3. Livingston, D. M., and Leder, P. (1969) *Biochemistry 8*, 435−443.
4. Takeda, M., and Webster, R. E. (1968) *Proc. Natl. Acad. Sci. U.S.A. 60*, 1487−1494.
5. Mazel, D., Pochet, S., and Marliere, P. (1994) *EMBO J. 13*, 914−923.
6. Rajagopalan, P. T. R., Yu, X. C., and Pei, D. (1997) *J. Am. Chem. Soc. 119*, 12418−12419.
7. Rajagopalan, P. T. R., Datta, A., and Pei, D. (1997) *Biochemistry 36*, 13910−13918.
8. Becker, A., Schlichting, I., Kabsch, W., Schultz, S., and Wagner, A. F. V. (1998) *J. Biol. Chem. 273*, 11413−11416.
9. Meinnel, T., Blanquet, S., and Dardel, F. (1996) *J. Mol. Biol. 262*, 375−386.
10. Chan, M. K., Gong, W. M., Rajagopalan, P. T. R., Hao, B., Tsai, C. M., and Pei, D. (1997) *Biochemistry 36*, 13904−13909.
11. Dardel, F., Ragusa, S., Lazennec, C., Blanquet, S., and Meinnel, T. (1998) *J. Mol. Biol. 280*, 501−513.
12. Hu, Y.-J., Rajagopalan, P. T. R., and Pei, D. (1998) *Bioorg. Med. Chem. Lett. 8*, 2479−2482.
13. Wei, Y., and Pei, D. (1997) *Anal. Biochem. 250*, 29−34.
14. Otwinowski, Z., and Minor, W. (1997) Methods Enzymol. *276*, 307−326.
15. Brunger, A. T. (1993) *X-PLOR Version 3.1 manual*, Yale University, New Haven, CT.
16. Jones, T. A., Zou, J. Y., Cowan, S. W., and Kjeldgaard, M. (1991) *Acta Crystallogr., Sect. A 47*, 110−119.
17. Brünger, A. T. (1993) *Acta Crystallogr., Sect. D 49*, 24−26.
18. McRee, D. E. (1993) *Practical Protein Crystallography*, Academic Press, Inc., San Diego.
19. Kraulis, P. (1991) *J. Appl. Crystallogr. 24*, 946−950.
20. Merritt, E., and Murphy, M. (1994) *Acta Crystallogr., Sect. D 50*, 869−873.
21. Laskowski, R. A., MacArthur, M. W., Moss, D. S., and Thornton, J. M. (1993) *J. Appl. Crystallogr. 26*, 283−291.

22. Kabsch, W., and Sander, C. (1983) *Biopolymers 22*, 2577−2637.
23. Lee, B., and Richards, F. M. (1971) *J. Mol. Biol. 55*, 379−400.
24. Tronrud, D., Holden, H., and Matthews, B. (1987) *Science 235*, 571−574.
25. Meinnel, T., Lazennec, C., and Blanquet, S. (1995) *J. Mol. Biol. 254*, 175−183.
26. Nicholis, A., Sharp, K., and Honig, B. H. (1991) *Proteins 11*, 281−296.

BI982594C